

Misfit strain–misfit strain diagram of epitaxial BaTiO₃ thin films: Thermodynamic calculations and phase-field simulations

G. Sheng,^{1,a)} J. X. Zhang,¹ Y. L. Li,¹ S. Choudhury,¹ Q. X. Jia,² Z. K. Liu,¹ and L. Q. Chen¹

¹Department of Materials Science and Engineering, The Pennsylvania State University, University Park, Pennsylvania 16802, USA

²MPA-STC, Los Alamos National Laboratory, Los Alamos, New Mexico 87545, USA

(Received 14 October 2008; accepted 6 November 2008; published online 11 December 2008)

The effect of anisotropic strains on the phase transitions and domains structures of BaTiO₃ thin films was studied using both thermodynamic calculations and phase-field simulations. The misfit strain–misfit strain domain stability diagrams were predicted. The similarity and significant differences between the diagrams from thermodynamic calculations assuming single domains and from phase-field simulations were analyzed. Typical domain structures as a result of anisotropic misfit strains are presented. © 2008 American Institute of Physics. [DOI: 10.1063/1.3039410]

Barium titanate is a classic oxide ferroelectric with the perovskite structure. It was the basis for the first generation of ceramic transducers and has wide applications in ceramic capacitors.¹ In the past two decades, there has been increasing interest in growing epitaxial BaTiO₃ thin films.^{2–5} The phase transition temperatures of BaTiO₃ thin films could be significantly increased by the misfit strains from the lattice and/or thermal expansion mismatches between the films and their substrates.^{3,6–8} A number of strain domain stability diagrams have been generated from thermodynamic calculations under a single domain assumption or assuming a simplified two-dimensional domain structure.^{2,4,9,10} Domain structures of BaTiO₃ thin films under isotropic biaxial strains were studied using the phase-field approach, and a “temperature–strain” phase diagram was constructed.¹¹ It was demonstrated that strain could also lead significant variations in the coercive fields of BaTiO₃ thin films.¹²

Epitaxial ferroelectric thin films are often grown on orthorhombic substrates such as GdScO₃ and NdGaO₃, which lead to an anisotropic in-plane misfit strain state.^{13–17} Therefore, it is desirable to investigate the effects of anisotropic misfit strains on the domain structures and properties of BaTiO₃ thin films. However, all the published diagrams^{18,19} under anisotropic strains were determined from thermodynamic analysis under a single domain assumption. Moreover, the sixth-order Landau–Devonshire potential²⁰ employed in these calculations limited the misfit strain to a relatively small compressive strains ($\leq \sim 0.4\%$).^{2,10,21} Recently, an eighth order potential²² was developed, which made it possible to construct strain stability diagrams under full range of anisotropic strains.

The phase-field approach has been employed to construct domain stability diagrams for PbTiO₃ thin films under anisotropic strains.²³ The obtained phase diagram shows significant difference from thermodynamic calculations. In this letter, we will report misfit strain–misfit strain diagrams from both thermodynamic calculations and phase-field simulations in BaTiO₃ thin films.

The properties of a BaTiO₃ single crystal bulk under stress-free condition are described by an eighth order polynomial in polarization components,²²

$$f_{\text{bulk}} = \alpha_1(P_1^2 + P_2^2 + P_3^2) + \alpha_{11}(P_1^4 + P_2^4 + P_3^4) + \alpha_{12}(P_1^2P_2^2 + P_2^2P_3^2 + P_3^2P_1^2) + \alpha_{111}(P_1^6 + P_2^6 + P_3^6) + \alpha_{112}[P_1^2(P_2^2 + P_3^2) + P_2^2(P_1^2 + P_3^2) + P_3^2(P_1^2 + P_2^2)] + \alpha_{123}P_1^2P_2^2P_3^2 + \alpha_{1111}(P_1^8 + P_2^8 + P_3^8) + \alpha_{1112}[P_1^6(P_2^2 + P_3^2) + P_2^6(P_1^2 + P_3^2) + P_3^6(P_1^2 + P_2^2)] + \alpha_{1122}(P_1^4P_2^4 + P_2^4P_3^4 + P_3^4P_1^4) + \alpha_{1123}(P_1^4P_2^2P_3^2 + P_2^4P_3^2P_1^2 + P_3^4P_1^2P_2^2), \quad (1)$$

where the spontaneous polarization vector $\mathbf{P}(\mathbf{x}) = (P_1, P_2, P_3)$, the coefficients α_{ij} , α_{ijk} , and α_{ijkl} are constants, and α_1 is linearly dependent on temperature.^{22,24}

When ferroelectric domains formed in a strained BaTiO₃ film, an elastic energy is generated and its density is given by

$$f_{\text{elas}} = \frac{1}{2}c_{ijkl}e_{ij}e_{kl} = \frac{1}{2}c_{ijkl}(\varepsilon_{ij} - \varepsilon_{ij}^0)(\varepsilon_{kl} - \varepsilon_{kl}^0), \quad (2)$$

where c_{ijkl} is the elastic stiffness tensor, e_{ij} and ε_{ij}^0 are the elastic strain and stress-free strain, respectively, and $\varepsilon_{ij} = e_{ij} + \varepsilon_{ij}^0$ is the total strain. Here, both ε_{ij} and ε_{ij}^0 are defined using the cubic phase as the reference, and $\varepsilon_{ij}^0 = Q_{ijkl}P_kP_l$, where Q_{ijkl} represents the electrostrictive coefficient.

In this work, a (001)-oriented BaTiO₃ thin film on an orthorhombic substrate is considered. A rectangular coordinate system $\mathbf{x} = (x_1, x_2, x_3)$ is set up with the x_1 , x_2 , and x_3 axes along the [100], [010], and [001] crystallographic directions, respectively. The average film/substrate misfit strains $e_{s1} = \bar{\varepsilon}_{11}$ and $e_{s2} = \bar{\varepsilon}_{22}$ along the in-plane x_1 and x_2 axes can be different. The details of the calculation of the total strain ε_{ij} are described in Refs. 25 and 26.

The thermodynamically most stable single-domain state is obtained by minimizing $f_{\text{bulk}} + f_{\text{elas}}$ under a given misfit strain and temperature. The materials constants at $T = 25$ °C are listed in Ref. 24. The corresponding “misfit strain–misfit strain” diagram assuming a single-domain state is shown in Fig. 1, with misfit strains ranging from -2% to 2% along both axes. We obtained seven stable single domain states. Three are tetragonal described by a_1 ($P_1 \neq 0$ and $P_2 = P_3 = 0$), a_2 ($P_2 \neq 0$ and $P_1 = P_3 = 0$), and c ($P_3 \neq 0$ and $P_1 = P_2 = 0$) and three are orthorhombic labeled as O_{12} ($P_1 \neq 0$, $P_2 \neq 0$, and $P_3 = 0$), O_{13} ($P_1 \neq 0$, $P_2 = 0$, and $P_3 \neq 0$), and O_{23} ($P_1 = 0$, $P_2 \neq 0$, and $P_3 \neq 0$), and the rhombohedral phase r ($P_1 \neq 0$, $P_2 \neq 0$, $P_3 \neq 0$). The rhombohedral phase is shown to be stable

^{a)}Electronic mail: shengguang@psu.edu.

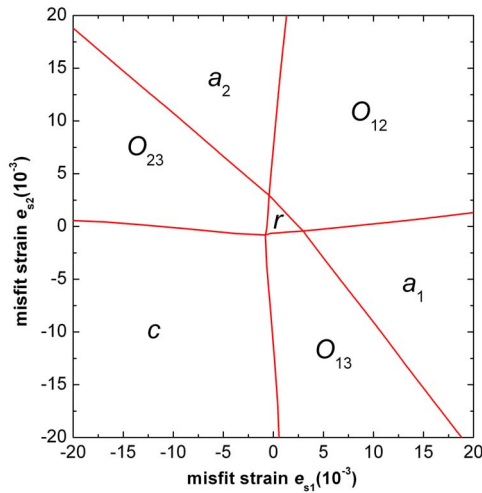


FIG. 1. (Color online) Misfit strain–misfit strain diagram of BaTiO₃ thin films at $T=25$ °C obtained by thermodynamic calculations.

near the center of this diagram in this work while its stability was not addressed in prior diagrams generated from the sixth-order potential.^{18,19} Our predicted diagram is, however, very similar to the recently reported diagram generated from the same thermodynamic potential.²⁷

To incorporate the possibility of multidomain and/or multiphase states in the phase diagram, we employed the phase-field approach by considering the polarization field as well as the local strain inhomogeneous. The temporal evolution of \mathbf{P} is governed by the time-dependent Ginzburg–Landau (TDGL) equations,

$$\frac{\partial P_i(\mathbf{x}, t)}{\partial t} = -L \frac{\delta F}{\delta P_i(\mathbf{x}, t)}, \quad i = 1, 2, 3, \quad (3)$$

where L is the kinetic coefficient and t is time. F is the total free energy given by

$$F = \int_V [f_{\text{bulk}}(P_i) + f_{\text{elas}}(P_i, \varepsilon_{ij}) + f_{\text{grad}}(P_{i,j}) + f_{\text{elec}}(P_i, E_i)] dV, \quad (4)$$

where V is the volume of the film, $f_{\text{grad}}(P_{i,j})$ and $f_{\text{elec}}(P_i, E_i)$ are the gradient energy and electrostatic energy densities, and $P_{i,j} = \partial P_i / \partial x_j$, E_i is the electric field. The calculation details of these energy terms are addressed in Ref. 28.

The temporal evolution of the polarization field and thus the domain structures are obtained by numerically solving the TDGL equations using the semi-implicit Fourier spectral method.²⁹ We employed a model of $128\Delta x \times 128\Delta x \times 36\Delta x$ grid size with periodic boundary conditions along the in-plane x_1 and x_2 axes. The thickness of the substrate and the film are taken as $h_s = 12\Delta x$ and $h_f = 20\Delta x$, respectively. Isotropic domain wall energy was assumed and the gradient energy coefficient $G_{11}/G_{110} = 1.0$, where G_{110} is related to the magnitude of Δx through $\Delta x = \sqrt{G_{110}/\alpha_0}$ and $\alpha_0 = |\alpha_1|_{T=25^\circ\text{C}}$. The initial polarization field is created by assigning a zero value at each cell plus a small random noise. The short-circuit boundary condition was employed.²⁸ Each simulation proceeded for 60 000 time steps (normalized time step is 0.05) until the polarization distribution achieved steadiness.

The misfit strain–misfit strain diagram constructed from the phase-field simulation is shown in Fig. 2. The thermodynamic diagram is also presented for comparison. It is noted

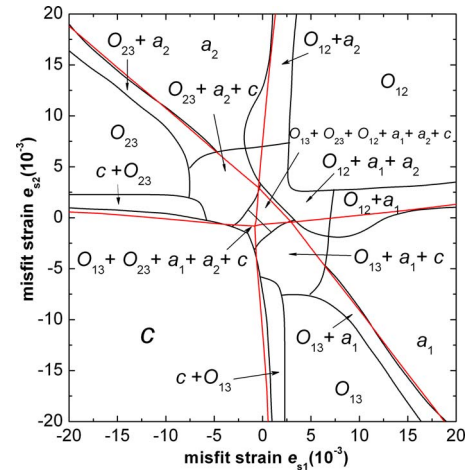


FIG. 2. (Color online) Misfit strain–misfit strain domain stability diagram for BaTiO₃ thin films at $T=25$ °C. The black lines are the phase boundaries from the phase-field simulations and the red lines are the ones from the thermodynamic calculations and the same as shown in Fig. 1.

that the domain stability diagram from the phase-field simulations is more complicated than that from the single-domain thermodynamic theory. It contains numerous regions of multidomain states. It is emphasized that although we use the same notations for domains or phases predicted from the thermodynamic theory and phase-field simulations (such as tetragonal c , a_1 , and a_2 or orthorhombic O_{12} , O_{13} , and O_{23}), the terminology “single phase” is used in the phase-field simulations to replace the “single domain” from the thermodynamic calculations. The difference is that each single phase obtained from phase-field approach always contains a mixture of equivalent polarization variants, for example, $(0, 0, P_3)$ and $(0, 0, -P_3)$ in pure c phase and $(+P_1, +P_2, 0)$, $(+P_1, -P_2, 0)$, and $(-P_1, +P_2, 0)$, and $(-P_1, -P_2, 0)$ in O_{12} phase. However, in thermodynamic analysis, the single domain region stands for one of the equivalent variants, such as single c domain stands for pure c^+ or c^- domain.

It is interesting to note that the diagram constructed from the phase-field approach has a stable binary phase region between every two neighbor single phase regions as a transitory area. Thus we have six regions of binary phases ($c+O_{13}$, $O_{13}+a_1$, a_1+O_{12} , $O_{12}+a_2$, a_2+O_{23} , and $O_{23}+c$). We also have three regions of three phase mixtures ($c+O_{13}+a_1$, $c+O_{23}+a_2$, and $O_{12}+a_1+a_2$) and two multiphase regions containing five and six phases near the center of the diagram, as shown in Fig. 2. The phase diagram from the phase-field approach is generated without any *a priori* assumption on the possible domain structures, and some of the domain structures are only close to the equilibrium state or may be even metastable. It is also noted that the diagonal of this diagram showing the domain configuration sequence as $c \rightarrow c+a_1+a_2+O_{13}+O_{23} \rightarrow c+a_1+a_2+O_{12}+O_{13}+O_{23} \rightarrow a_1+a_2+O_{12} \rightarrow O_{12}$, which is also consistent with the “strain-temperature” diagrams from our previous simulations.¹¹

Examples of domain structures from the simulations are shown in Figs. 3 and 4. Different domain variants are identified by colors and labeled in the figures. Figure 3(a) exhibits a typical tetragonal domain structure under large compressive strains for both x_1 and x_2 directions ($e_{s1} = e_{s2} = -0.010$), in which there are two types of c domains of $(0, 0, P_3)$ and $(0, 0, -P_3)$ separated by 180° domain walls. Single a_1 phase [Fig. 3(b)] is stable only when a large tensile strain is applied

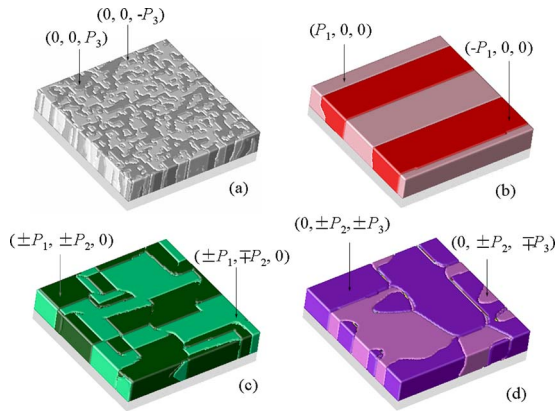


FIG. 3. (Color online) Typical domain structures of single phase in BaTiO₃ thin films. (a) Tetragonal c domains at $e_{s1}=e_{s2}=-0.010$. (b) Tetragonal a_1 domains at $e_{s1}=0.015$ and $e_{s2}=-0.010$. (c) Orthorhombic O_{12} domains at $e_{s1}=e_{s2}=0.015$. (d) Orthorhombic O_{23} domains at $e_{s1}=-0.015$ and $e_{s2}=0.005$.

at the x_1 axis and a large compressive strain is at the x_2 axis. Figure 3(c) is the general orthorhombic O_{12} domain structure with large tensile strains applied on both axes (here $e_{s1}=e_{s2}=0.015$). Figure 3(d) is another interesting domain structure induced by anisotropic strains. When choosing an appropriate tensile strain along one axis and compressive strain along the other, we can get the pure O_{13} or O_{23} phases. To simplify the exhibition of domain structure in orthorhombic domains, we only identify in Fig. 3(d) the two types of O_{23} domains $[(0, \pm P_2, \pm P_3)$ and $(0, \pm P_2, \mp P_3)]$ instead of all four variants ($e_{s1}=-0.015$ and $e_{s2}=0.005$). The same treatment is applied to O_{12} and O_{13} domains. Figures 4(a)–4(f)

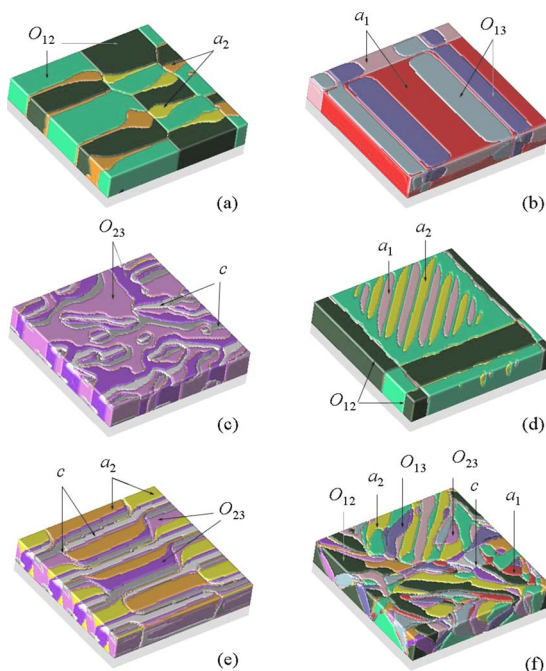


FIG. 4. (Color online) Typical multidomain structures in BaTiO₃ thin films. (a) Tetragonal a_2 + orthorhombic O_{12} domains at $e_{s1}=0.00125$ and $e_{s2}=0.010$. (b) Tetragonal a_1 + orthorhombic O_{13} domains at $e_{s1}=0.00875$ and $e_{s2}=-0.010$. (c) Tetragonal c + orthorhombic O_{23} domains at $e_{s1}=-0.0125$ and $e_{s2}=-0.00125$. (d) Tetragonal a_1+a_2 + orthorhombic O_{12} domains at $e_{s1}=e_{s2}=0.002$. (e) Tetragonal c + tetragonal a_2 + orthorhombic O_{23} domains at $e_{s1}=-0.00375$ and $e_{s2}=0.00125$. (f) Multidomain structure containing all the above domains at $e_{s1}=e_{s2}=0.0005$.

are the multidomain structures containing at least two phases.

In summary, the misfit strain–misfit strain phase/domain stability diagram was constructed for BaTiO₃ thin films at room temperature using both thermodynamic calculations and phase-field simulations. It is expected that such diagrams will provide guidance for interpreting experimental measurements and observations as well as to the design of BaTiO₃ films with specified domain structures.

This work was supported by the DOE under Grant No. DOE DE-FG02-07ER46417, NSF through Grant Nos. DMR-0507146 and DMR-0820404, and the Los Alamos National Laboratory supported by DOE through the LANL/LDRD Program (Q.X.J.). The computer simulations were carried out on the LION clusters at the Pennsylvania State University supported in part by the Materials Simulation Center and the Graduate Education and Research Services at PSU.

¹G. Haertling, *J. Am. Ceram. Soc.* **82**, 797 (1999).

²N. A. Pertsev, A. G. Zembilgotov, and A. K. Tagantsev, *Phys. Rev. Lett.* **80**, 1988 (1998).

³K. J. Choi, M. Bieganski, Y. L. Li, A. Sharan, J. Schubert, R. Uecker, P. Reiche, Y. B. Chen, X. Q. Pan, V. Gopalan, L. Q. Chen, D. G. Schlom, and C. B. Eom, *Science* **306**, 1005 (2004).

⁴O. Dieguez, S. Tinte, A. Antons, C. Bungaro, J. B. Neaton, K. M. Rabe, and D. Vanderbilt, *Phys. Rev. B* **69**, 212101 (2004).

⁵M. Jimi, T. Ohnishi, K. Terai, M. Kawasaki, and M. Lippma, *Thin Solid Films* **486**, 158 (2005).

⁶D. G. Schlom, L. Q. Chen, C. B. Eom, K. M. Rabe, S. K. Streiffner, and J.-M. Triscone, *Annu. Rev. Mater. Res.* **37**, 589 (2007).

⁷L. Q. Chen, *J. Am. Ceram. Soc.* **91**, 1844 (2008).

⁸D. G. Schlom, L. Q. Chen, X. Q. Pan, A. Schmehl, and M. A. Zurbuchen, *J. Am. Ceram. Soc.* **91**, 2429 (2008).

⁹N. A. Pertsev and V. G. Koukhar, *Phys. Rev. Lett.* **84**, 3722 (2000).

¹⁰V. G. Koukhar, N. A. Pertsev, and R. Waser, *Phys. Rev. B* **64**, 214103 (2001).

¹¹Y. L. Li and L. Q. Chen, *Appl. Phys. Lett.* **88**, 072905 (2006).

¹²S. Choudhury, Y. L. Li, L. Q. Chen, and Q. X. Jia, *Appl. Phys. Lett.* **92**, 142907 (2008).

¹³Y. Lin, X. Chen, S. W. Liu, C. L. Chen, J.-S. Lee, Y. Li, Q. X. Jia, and A. Bhalla, *Appl. Phys. Lett.* **84**, 577 (2004).

¹⁴A. G. Zembilgotov, N. A. Pertsev, U. Böttger, and R. Waser, *Appl. Phys. Lett.* **86**, 052903 (2005).

¹⁵W. K. Simon, E. K. Akdogan, and A. Safari, *J. Appl. Phys.* **97**, 103530 (2005).

¹⁶W. K. Simon, E. K. Akdogan, and A. Safari, *Appl. Phys. Lett.* **89**, 022902 (2006).

¹⁷G. Akcay, I. B. Misirlioglu, and S. P. Alpay, *J. Appl. Phys.* **101**, 104110 (2007).

¹⁸J. Wang and T. Y. Zhang, *Appl. Phys. Lett.* **86**, 192905 (2005).

¹⁹J. H. Qiu and Q. Jiang, *J. Appl. Phys.* **101**, 034110 (2007).

²⁰A. J. Bell and L. E. Cross, *Ferroelectrics* **59**, 197 (1984).

²¹D. A. Tenne, X. X. Xi, Y. L. Li, L. Q. Chen, A. Soukiassian, M. H. Zhu, A. R. James, J. Lettieri, D. G. Schlom, W. Tian, and X. Q. Pan, *Phys. Rev. B* **69**, 174101 (2004).

²²Y. L. Li, L. E. Cross, and L. Q. Chen, *J. Appl. Phys.* **98**, 064101 (2005).

²³G. Sheng, J. X. Zhang, Y. L. Li, S. Choudhury, Q. X. Jia, Z. K. Liu, and L. Q. Chen, *J. Appl. Phys.* **104**, 054105 (2008).

²⁴ $\alpha_1=4.124(T-115)\times 10^5$, $\alpha_{11}=-2.097\times 10^8$, $\alpha_{12}=7.974\times 10^8$, $\alpha_{111}=1.294\times 10^9$, $\alpha_{112}=-1.950\times 10^9$, $\alpha_{123}=-2.500\times 10^9$, $\alpha_{1111}=3.863\times 10^{10}$, $\alpha_{1112}=2.529\times 10^{10}$, $\alpha_{1122}=1.637\times 10^{10}$, $\alpha_{1123}=1.367\times 10^{10}$, $c_{11}=1.78\times 10^{11}$, $c_{12}=0.964\times 10^{11}$, $c_{44}=1.22\times 10^{11}$, $Q_{11}=0.10$, $Q_{12}=-0.034$, and $Q_{44}=0.029$ in SI units and T in °C.

²⁵Y. L. Li, S. Y. Hu, Z. K. Liu, and L. Q. Chen, *Acta Mater.* **50**, 395 (2002).

²⁶Y. L. Li, S. Y. Hu, Z. K. Liu, and L. Q. Chen, *Appl. Phys. Lett.* **78**, 3878 (2001).

²⁷A. G. Zembilgotov, U. Böttger, and R. Waser, *J. Appl. Phys.* **104**, 054118 (2008).

²⁸Y. L. Li, S. Y. Hu, and L. Q. Chen, *J. Appl. Phys.* **97**, 034112 (2005).

²⁹L. Q. Chen and J. Shen, *Comput. Phys. Commun.* **108**, 147 (1998).